Cross-linked Polymersome Membranes: Vesicles with Broadly Adjustable Properties

Bohdana M. Discher,† Harry Bermudez,† Daniel A. Hammer, and Dennis E. Discher*

School of Engineering and Applied Science, University of Pennsylvania, Philadelphia, Pennsylvania 19104

You-Yeon Won and Frank S. Bates

Department of Chemical Engineering and Materials Science, University of Minnesota, Minneapolis, Minnesota 55455

Received: May 22, 2001; In Final Form: December 20, 2001

Massively cross-linked and property-tunable membranes have been fabricated by free radical polymerization of self-assembled, block copolymer vesicles − polymersomes. Similar efforts with cross-linkable lipids would appear frustrated in the past due to at least two factors: limited reactivity and membrane fragility under local stresses of nano-confined cross-linking. We describe here a diblock copolymer of poly(ethylene oxide)-polybutadiene that has a hydrophilic weight fraction like that of lipids and forms robust fluid phase membranes in water. The polymersomes sustain free radical polymerization of the hydrophobic butadiene, thereby generating a semipermeable nano-shell. Cross-linked giant vesicles prove stable in chloroform and can also be dehydrated and re-hydrated without rendering the ~9 nm thick membrane core; the results imply defect-free membranes many microns-squared in area. Surface elastic moduli as well as sustainable wall stresses up to 10^3 Atm, orders of magnitude greater than any natural lipid membrane, appear consistent with strong tethering between close-packed neighbors. The enormous stability of the giant vesicles can be tuned down for application: blending in the hydrogenated analogue poly(ethylene oxide)-polyethylethylene modulates the effective elastic constants as well as the rupture strength by orders of magnitude. The results appear consistent with rigidity percolation through a finite-layer stack of two-dimensional lattices. Moreover, below the percolation limit, a regime of hyper-instability emerges, reflecting perhaps nanoscale demixing and suggestive of the limitations encountered with low reactivity lipids. The results provide general insights into covalent cross-linking within self-assembled nanostructures.

Introduction

Covalent cross-linking of polymeric assemblies is not only a long-accepted means of bulk stabilization, but also is a rapidly emerging approach to bridging the nanoscale world of labile, interfacially driven self-assemblies with the meso-scale. As prime examples of massively cross-linked structures, giant nanorods many microns in length have been reported for at least two block copolymer systems.[1,2] Free-radical cross-linking of EO_m-BD_n ($m = 55$, $n = 45$) has been shown, in aqueous dispersions, to give a considerably more elastic material than rods of the non-crosslinked precursor. Aligned nanowire arrays[3] and optically patterned thin film mesophases[4] are two additional examples of self-assemblies that are driven to assemble via polymeric surfactancy and subsequently stabilized by cross-linking. However, assessing the material nature of inner-polymerized nanostructures, with elastic and stability properties no longer dominated by fluid interfaces, can prove a challenge. Simple observations of morphology or tests of solubilization and heat stability generate initial benchmarks, but generally provide little to no insight into critical issues such as polymerization-induced strains[2] and defects that limit stability.

Membranes, particularly those that define and delimit vesicles, can serve as sensitive and accessible model systems for understanding many such nano-structure/response relationships.[5] Lipid membrane stabilization through polymerization has been investigated for many years [6,7] and to some extent been established in a range of submicron vesicle systems. For example, small vesicles with a high degree of polymerization that opposes detergent induced leakage of entrapped solutes have been recently made by O'Brien and co-workers.[8] However, many years of effort suggest that the requisite 2-*D*-reaction is difficult to propagate without the induction of membrane curvature, defects, and rendering over supramolecular length scales.[10,11] Nonetheless, some pure and mixed component small vesicle systems are beginning to find use in applications such as oral drug delivery.[9]

An increasing realization of the need for enhanced reactivity[12,13] underscores the limits imposed by "small", lipid-size membrane constituents. More massive block copolymers considerably broaden the general synthetic approach. In purely aqueous solutions, several di- and tri-blocks have now been shown capable of self-assembly into "polymersomes" that range from nanoscale[14,15] to cell-sized giant vesicles with thick as well as extraordinarily tough membranes.[16,17] As a consequence of the increased membrane thickness, copolymers that are now also made to be cross-linkable such as the poly(ethylene oxide)-polybutadiene (PEO−PBD) diblock elaborated here, necessarily contain many more reactive groups than can be designed into lipids. Cross-linkable block copolymers, with their intrinsic toughness and high reactivity, are thus predisposed to the generation of extremely stable, supramolecular surfaces.

The nature of the chemical cross-linking and the new physical properties that arise at the nanoscale are of broad relevance. Giant vesicles reported here offer an alternative and more direct route to understanding meso-material relations. Nanoscale relations between cross-link arrangement and micellar properties would seem difficult to elucidate except through a heavy reliance

* To whom correspondence should be addressed. E-mail: discher@seas.upenn.edu.

† Equal contributors to this work.

10.1021/jp011958z CCC: $22.00
Published on Web 02/26/2002

on theoretical models of *bulk* response such as those developed for filamentous actin.[18] With the newly developed vesicular systems, various tests of membrane permeation provide molecular-scale insights into defect density, whereas morphological clues that span many length scales generate insights into cross-linking efficiency. Because the micron-size surfaces can be directly characterized by methods of controlled manipulation,[16] cross-link-dependent measures of mechanical properties can be obtained. Polymerization phenomena ranging from 2-*D* rubber elasticity to bond percolation through a non-crosslinkable matrix are thus made accessible, with broad and general implications to mesophase stabilization. Moreover, specific property comparisons are fruitfully made with naturally occurring laterally cross-linked structures, notably the spectrin skeleton of the red cell plasmalemma. This cell biological structure has clearly been shown critical to biomembrane stability[19] and has also long motivated synthetic efforts at mimicry[20] of the general type illustrated here.

Experimental Methods

Block copolymers were synthesized by anionic polymerization as described elsewhere.[2,17] Vesicles form spontaneously upon hydration of either bulk copolymer or dried films of copolymer obtained after chloroform evaporation. Aqueous solutions range from pure water to sucrose solutions of 300 mOsm to phosphate-buffered saline. Polybutadiene in the cores of the vesicle membranes was cross-linked by free radical polymerization in solution, following Won and co-workers,[2] with the radicals generated through a $K_2S_2O_8$ initiator and a redox couple, $Na_2S_2O_5/FeSO_4 \cdot 7H_2O$. The osmolarity was balanced so as not to rupture the vesicles during addition of these reagents. As described later, the extent of reaction was established by measuring changes in membrane rupture tension. This and additional mechanical properties of polymersome membranes, either fully cross-linked or not, were obtained (at ≈23 °C) by micropipet aspiration.[16]

Results

Giant unilamellar vesicles form spontaneously when slivers of bulk $EO_{26}-BD_{46}$ (designated **OB2**) are added to aqueous solutions (Figure 1A). Such vesicles exhibit several characteristics indicative of a fluid-phase membrane. First, when sheared from their substrate and isolated, vesicles transform morphologically with smooth contours (Figure 1B). Second, like any lipid bilayer, these uncross-linked **OB2** vesicles dissolve readily when a good solvent such as chloroform is added at only a fraction of a percent. Each molecule in the self-assembled vesicle contains a hydrophobic block with, on average, 46 double bonds that are readily available for cross-linking by common means of solution polymerization. When the giant polymersome vesicles are exposed to free radicals in an osmotically balanced medium, massive cross-linking is achieved. The membrane transformation from liquid to solid state is directly observable upon osmotic deflation of the originally spherical vesicle as creases, folds, wrinkles, and dents proliferate (Figure 1C). Like the deflation of a micron-sized rubber ball, these features reflect the fact that molecules cannot significantly rearrange within the surface to relax accumulated strain.[21] At the same time, phase contrast images clearly demonstrate membrane integrity through sustained retention of small molecule encapsulants such as sucrose (Figure 1C). Vesicle shape as well as membrane thickness are minimally affected by the cross-linking reagents or the reaction process itself as long as solution osmolarity is held constant.

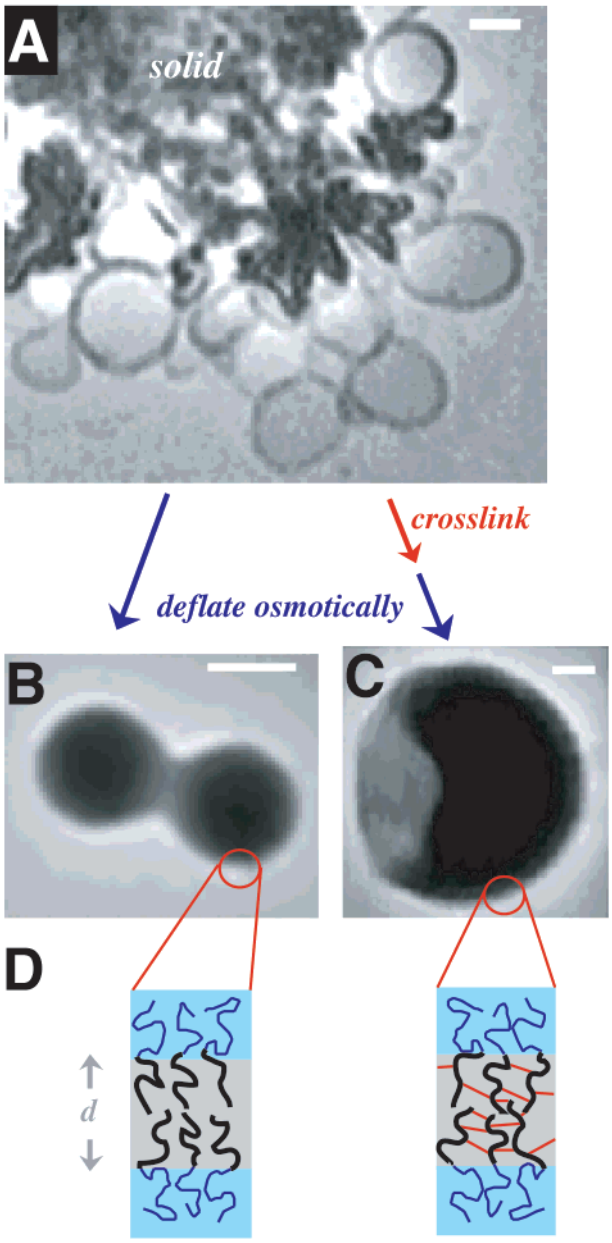

Figure 1. Formation and osmotic deflation of **OB2**, i.e., $(EO)_{26}-(BD)_{46}$, vesicles either without (A, B) or with (C) cross-linking between the hydrophobic segments of butadiene. (A) Brightfield image of bulk copolymer hydrating and vesiculating into a 200 mOsm sucrose solution. Giant, spherical, unilamellar vesicles predominate. The scale bars for A, B, and C are all 5 μm. Separate cryo-TEM images show the hydrophobic core thickness to be $d = 9 \pm 1$ nm.[26] (B) Dilution into 300 mOsm phosphate-buffered saline (PBS) increases the internal osmotic pressure by deflating a spherical, non-crosslinked vesicle. A smooth vesicle contour is generated, and the refractive index difference between sucrose and PBS makes vesicles appear dark in phase contrast imaging, proving the integrity of the vesicle's membrane. (C) When cross-linked and subsequently diluted into PBS, the vesicle deflates with dents and wrinkles, characteristic of a solidlike membrane. (D) Illustrative schematics of the diblock copolymer membranes, showing a close-packed arrangement of copolymers with a hydrophobic core thickness *d*.

Cross-linked polymersomes were first tested for stability in chloroform ($CHCl_3$), an excellent solvent for **OB2**. Transfer of a single vesicle into $CHCl_3$ from phosphate-buffered saline (PBS) shows no alteration of vesicle size, shape, volume, or area for as long as the vesicle was held in solvent (Figure 2A). If chloroform were to significantly swell the hydrophobic core without being strongly opposed by intramembrane cross-linking,

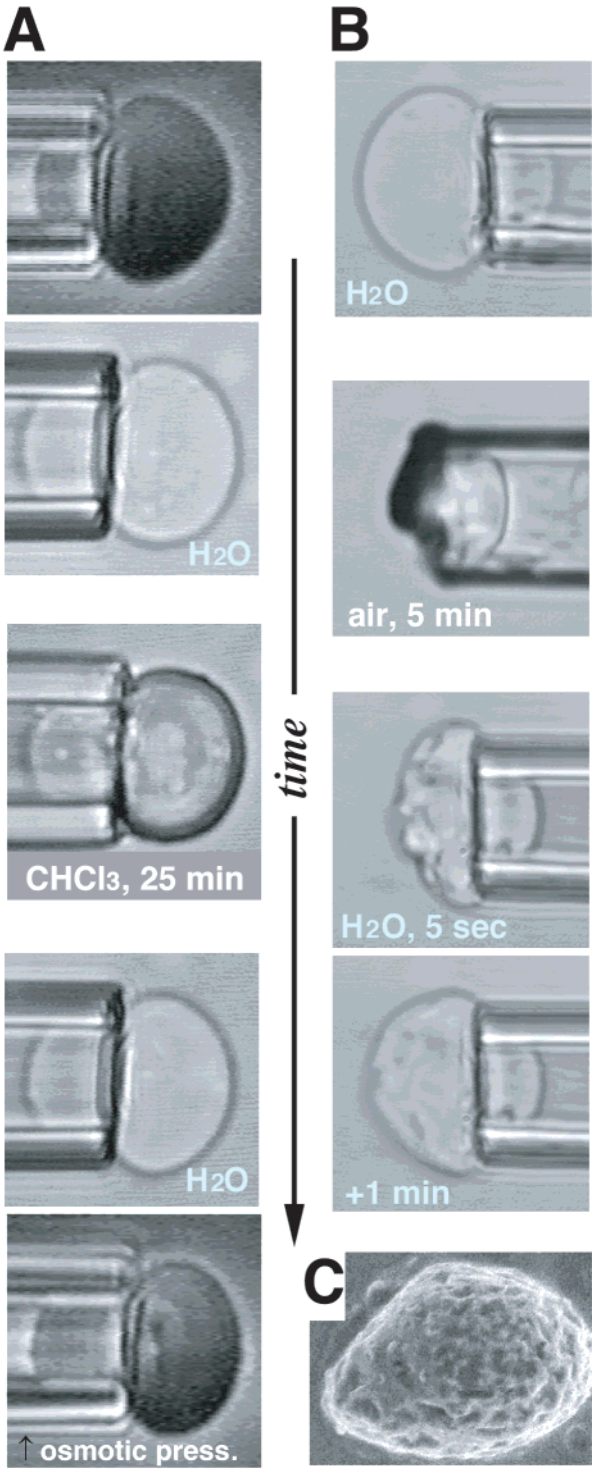

Figure 2. Stability of individual vesicles of cross-linked **OB2** during transfer into chloroform (A), air (B), or vacuum (C). (A) The top two images show a sucrose-containing vesicle held by a micropipet (of inner radius $R_P = 4.8$ μm) in PBS solution and viewed in phase contrast (dark) or brightfield. The middle image shows a vesicle transferred into chloroform and held there for 30 min, followed by transfer back into aqueous solution. Sucrose retention is visually obvious from the phase contrast in the first and last images. This is confirmed by the last image which shows the expected decrease in vesicle volume when the exterior osmolarity is increased. (B) A vesicle in aqueous solution pulled into a micropipet ($R_P = 4.2$ μm) and then removed from the chamber and imaged within seconds after exposure to air. Rehydration occurs immediately upon reinsertion of the vesicle back to the aqueous solution. (C) Scanning electron micrograph of a vesicle prepared simply by vacuum-drying without staining or fixation. The long axis of the vesicle is 10 μm.

the aspirated projection of the vesicle would have lengthened with the increase in membrane area. This is not observed. Moreover, upon transferring the vesicle back to aqueous solution, the vesicle's geometry is unaffected, indicative of full retention of the encapsulated solute, sucrose. Loss of even a few weight percent sucrose from the vesicle into the chloroform would again have lengthened the aspirated projection due to a decrease in vesicle volume during osmotic equilibration.[16] This principle, along with a finite permeability of the cross-linked membrane to water, is illustrated in the bottom panel of Figure 2A through a final increase in external solute concentration. The encapsulated sucrose is still retained inside the vesicle as again directly imaged by phase contrast microscopy using the refractive index difference between the interior sucrose and the exterior PBS. Stability and integrity of the cross-linked membrane down to the molecular scale are thus confirmed.

Cross-linked **OB2** membranes were next tested for stability through a simple cycle of dehydration−rehydration. A vesicle aspirated into a micropipet is pulled out of aqueous solution (Figure 2B), across the water−air interface. As the picoliters of encapsulated water evaporate through the increasingly wrinkled membrane, the vesicle collapses. Subsequent return of the semi-dehydrated vesicle to aqueous solution leads, however, to rapid rehydration and vesicle swelling as illustrated in the bottom panel of Figure 2B. The phase contrast again indicated retention of encapsulated solutes. Similar experiments in bulk show that cross-linked vesicles can be dried, stored at room temperature for days and then rehydrated to their original average diameter and volume. Vacuum drying allows direct imaging by scanning electron microscopy which reveals, at high resolution, the cross-corrugated surface texture of a vacuum-dried vesicle (Figure 2C).

Quantitative analysis of the effective Laplace tension, τ, induced by aspiration (e.g., Figure 2A,B) demonstrates the tremendous increase in elastic stiffness and mechanical stability achieved by full, covalent cross-linking of an **OB2** vesicle (Figure 3). Prior to cross-linking, **OB2** vesicles respond in a manner generic to fluid phase membranes: they resist aspiration in close proportion to the same interfacial tension, γ, that drives their self-assembly.[22] Thus, like a soap bubble in air, pressurization spheres the outer contour of the fluid vesicle (Figure 3B lower inset) and homogeneously dilates the membrane's area. The slope of τ versus relative area yields K_a ($=4\gamma$) of 107 ± 14 mN/m (9 vesicles).

Upon cross-linking in a flaccid state (Figure 3A), **OB2** membranes clearly respond with a more solidlike character in deformation. When aspirated sufficiently, the vesicle contour immediately outside of the micropipet clearly appears flattened (Figure 2A, B) relative to a sphere (Figure 3B, lower inset). In this same flattened region, brightfield imaging often shows corrugations of buckled membrane radiating away from the micropipet entrance (Figure 3C). These folds are especially apparent in fluorescence imaging when using labeled **OB2** and pressurized vesicles (Figure 3B, upper inset). Analogous to corrugations in cardboard, radial folds in this region would tend to stiffen against bending and should thus flatten the membrane. Prior to buckling, the deformation is largely reversible and effectively elastic; the wrinkles or folds tend to protract relaxation, however. Related to the effective elasticity and elaborated upon in the Discussion, plots of the effective tension τ against the extensional strain measure $x = L/R_p$ generally leads to three quasi-linear regimes labeled in Figure 3B. Importantly, the strain measure x is not the relative area change which is used to obtain K_a. The straining process is more anisotropic

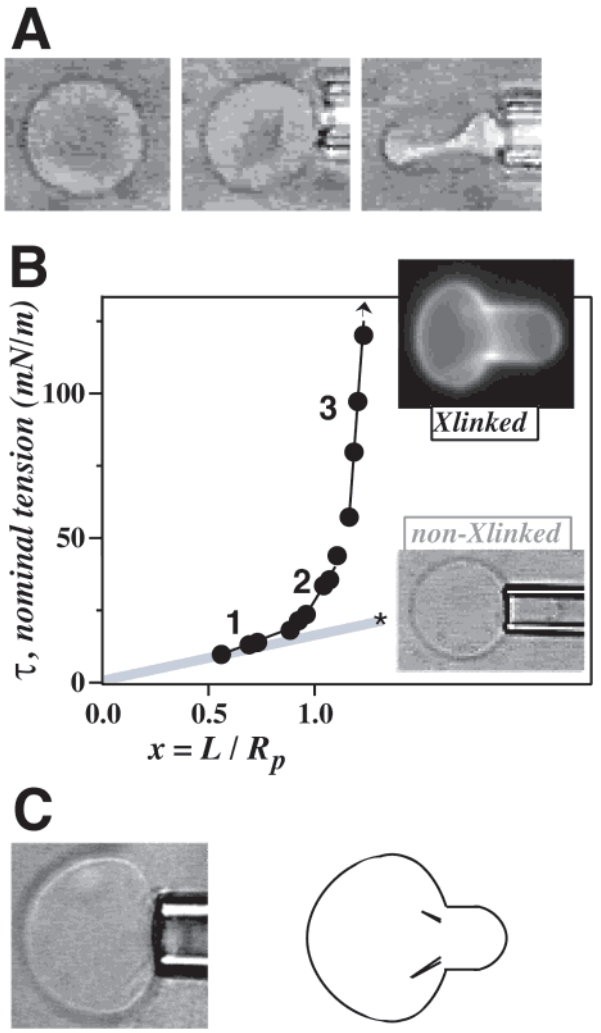

Figure 3. Deformability of cross-linked **OB2** vesicles in comparison with non-crosslinked **OB2**. (A) Viewed in brightfield, this **OB2** vesicle was cross-linked in a highly deflated (nonspherical) state. Manipulative rotation using a micropipet shows a dimpled, red cell-like, or discocyte shape. (B) Further aspiration of a similar vesicle generates a nominal membrane tension, τ, in the aspirated direction which is proportional to the applied pressure but nonlinear with the extension of the membrane, L, into the pipet. This depends on the compliant nature of the membrane as well as on the vesicle's volume, V, relative to the volume of a sphere, V_{MAX}, of the same area. Three regimes of aspiration are typically found for a flaccid vesicle ($V < V_{MAX}$). At small extension (denoted regime 1), the membrane appears to seal against the micropipet as large "dents", typically smaller than the discocyte's dimple, are smoothed out. At intermediate extension (regime 2: $L \approx R_P$), the outer vesicle contour appears more axisymmetric with the membrane forced to constrict upon entering the pipet; this is the regime most readily identified with membrane shearing. In a final high pressure regime 3, extension into the micropipet is minimal while wrinkles appear locked in by contact with the micropipet wall. The upper inset image highlights such wrinkles emanating from the mouth of the pipet on a fluorescently labeled, cross-linked vesicle. In comparison, non-crosslinked **OB2** vesicles exhibit more linear aspiration curves (gray line); and the tensions at rupture for such fluid membranes are orders of magnitude smaller than the ≈1000 mN/m tensions sustainable by cross-linked membranes. The lower inset image shows a non-crosslinked vesicle in aspiration and illustrates the spherical contour of membrane outside of the micropipet, consistent with an isotropically tensed fluid membrane. (C) Brightfield imaging of cross-linked vesicles in aspiration often shows membrane wrinkles as well. The sketch at right with two V-shaped wrinkles provides a guide to the eye for the particular image shown. R_P in all of the images range from 3 to 5 μm.

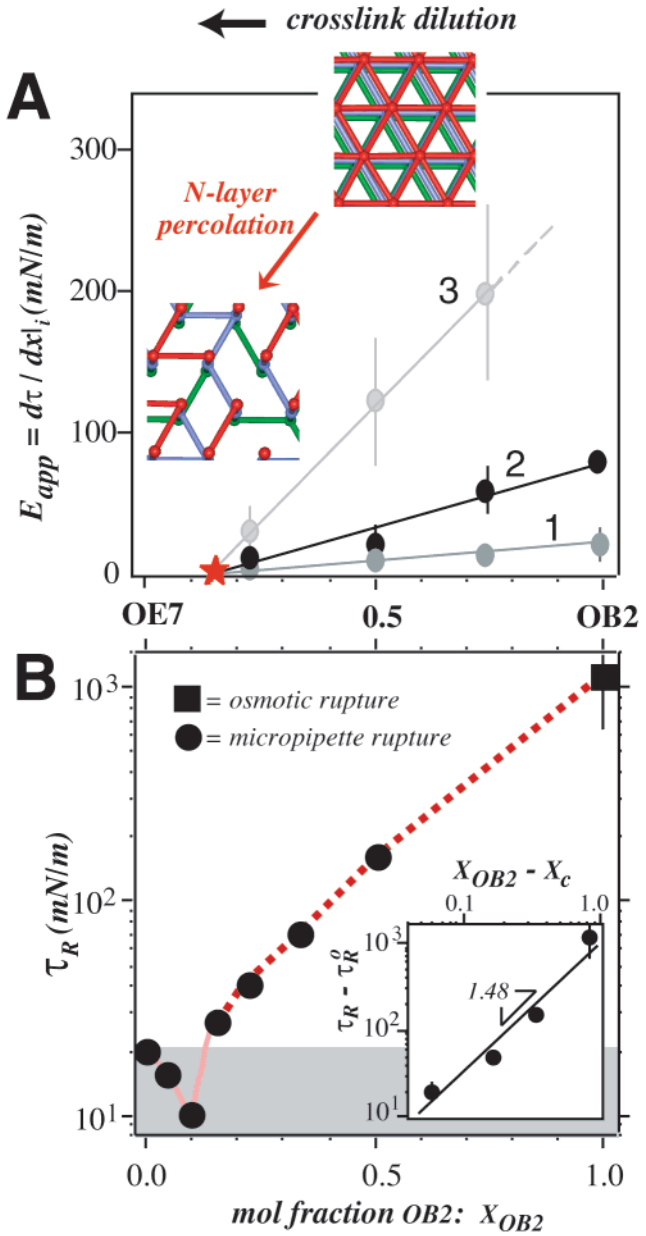

Figure 4. Elasticity and mechanical stability of cross-link-diluted **OB2** vesicles made by blending in varying molar ratios of the non-crosslinkable analogue **OE7**. (A) Three effective elastic constants were deduced from the three regimes of aspiration illustrated in Figure 3B. The three elastic constants appear to scale linearly with cross-link dilution above a critical fraction of **OB2**. Linear fits all intersect at a mole fraction of $X_{OB2} = 16 \pm 2\%$ near $E_{app} = 0$. (B) The effective rupture tension, τ_R, is a more nonlinear function of cross-link dilution. Above $X_{OB2} \approx 15\%$ ($\equiv X_C$), τ_R increases monotonically with weak power-law scaling (lower inset). Below X_C, τ_R exhibits a minimum: the entire gray region highlights cross-link-induced destabilization. Importantly, the cross-linking reaction does not alter the previously reported value of $\tau_R{}^o$ for a pure **OE7** system. In addition, we followed the kinetics of all cross-linking reactions through measurements of τ_R and find that polymerizations are complete within 10 min of initiation; values of τ_R reported here correspond to end-point measures. Each data point represents an average ($\pm$ S.D.) of measurements on at least 3 vesicles.

and less homogeneous. The slope for each of the three quasi-linear regimes nonetheless provides phenomenological measures of membrane bending, shear, and dilational resistance. Figure 4A summarizes these measures as apparent moduli for fully cross-linked **OB2** membranes as well as the cross-link-diluted systems elaborated below.

The remarkable stability of a cross-linked versus a non-crosslinked membrane (Figure 3B) motivates a chemically

controllable approach to property modulation. The fully hydrogenated homologue of **OB2** is the copolymer poly(ethylene oxide)-polyethylethylene ($EO_{40}-EE_{37}$ designated **OE7**).[23] **OB2** and **OE7** membranes exhibit nearly identical K_a's.[16] The implication of this is useful and important: since $K_a \sim \gamma$ and $\gamma^2 \sim \chi$, i.e., the dominant Flory interaction parameter χ that drives self-assembly,[24] **OB2** and **OE7** have measurably identical chemistries and therefore ought to be largely miscible. The miscibility of **OE7** with **OB2** has indeed been confirmed by imaging vesicles containing fluorescently tagged copolymers. Blending followed by cross-linking therefore provides a means of modulating membrane properties through partial cross-linking. Dilution of cross-linked **OB2** by blending in **OE7** clearly reduces the apparent stiffnesses of the composite membrane. As might be expected, above some apparent critical concentration of bonds, the elasticity is reduced in linear relation to the cross-linkable mole fraction $X(=X_{OB2})$ (Figure 4A).

Mixed and cross-linked membranes with X below some apparent critical concentration X_C ($\approx$16%) of **OB2** are less stable under stress (Figure 4B). Indeed, the apparent rupture tension τ_R is seen to cross below the baseline value set by pure non-crosslinkable membranes, reaching a minimum measured value near $X \approx 10\%$ that is almost 3-fold below baseline (i.e., τ_R of **OE7**). This destabilization is generally reminiscent of that seen with polymerizable lipids,[10,11] but structural clues of mechanism are not readily apparent. Images of fluorescently labeled mixtures generally yield a homogeneous membrane (see inset to Figure 3C), indicating that, even within the few minutes of the free radical reaction, cross-linking is homogeneous on an optical scale of hundreds of nanometers. The homogeneity suggests that nanometer scale phenomena such as polymerization induced strains weaken the membrane. Contrary to the destabilization of the membrane with constituent-limited polymerization, full cross-linking of 100% **OB2** corresponds to an extremely large rupture stress across the membrane: $\tau_R/d \approx$ 1000 Atm, which is estimated from osmotic swelling and rupture experiments. This proves mechanically consistent with cross-link stabilization of the membrane because phospholipid membranes[25] as well as non-crosslinked polymer membranes rupture in the range of $\tau_R/d \approx 10-50$ Atm. As discussed below, the various results can be used for further theoretical analysis of the cross-linking reaction and emergent properties.

Discussion

In comparison to a critical strain of 5% or less that is *universal* to lipid membranes,[26] polymersome membranes can withstand dilational strains of almost 20% before rupture. Transverse strains that arise with free-radical cross-linking and which thin the hydrophobic core by about 10%[27,2] can thus be withstood. The result is that these micron-sized nano-structures of copolymer consistently (and uniquely) survive cross-linking. Consistent with this, phase contrast images (Figure 2A) clearly demonstrate membrane integrity through sustained retention of small molecule encapsulants. Such a separation of solutes further implies a close-packed (i.e., quasi-hexagonal) arrangement of amphiphiles in the membrane. Dense cross-linking between molecules so arranged is expected to produce a thin solidlike shell that not only resists harsh environmental changes, such as drying (Figure 2B, C), but also exhibits classic surface elastic, rather than fluid lipid membrane − characteristics in deformation.

Assuming an isotropicaly cross-linked shell, the strain energy is expected to be stored locally as both in-plane stretching and bending.[28] Whereas the energy scale for stretching is set by the cross-linked butadiene of intrinsic shear modulus $\mu_{3D} \approx \mu_{2D}/d$, the energy scale for bending is also set by the thickness in terms of a bending modulus $K_b \sim \mu_{2D}d^2$. Compared to inflation of an air bubble in water which invariably displays a smoothly tensed interface, the curved and undulating surface of the sort illustrated in osmotic re-inflation of a dried, cross-linked vesicle (Figure 2B at 5 s) is highly suggestive of a finite K_b, Thus, given the relations above, a finite shear modulus is not only expected but likely to be revealing of intrinsic features of the cross-linked butadiene.

Effective Elastic Moduli. In aspiration of slightly deflated cross-linked vesicles, bending and stretching are again expected to be prominent and, we propose, they contribute to distinct regimes of stressing these shell-like structures. Indeed, three quasi-linear regimes of aspiration were typically identified, contrasting considerably with the simpler aspiration of an isotropic fluid membrane which is homogeneously stressed in aspiration (Figure 3B). Analyses of the two sorts of membranes—fluid or solid—are distinct, but largely worked out for the red cell membrane which behaves as a fluid-solid composite.[29] In aspiration of this cell, the lipid bilayer initially resists bending before the underlying spectrin network contributes a shear resistance at more modest pressures. At higher pressures, a buckling instability leads to membrane folds which, because of bilayer fluidity, are smoothed out at the highest pressures where the cohesiveness of the lipid resists rupture. A lack of fluidity in the covalently cross-linked membranes here appears to produce only slightly different behavior. Regime #1, at the lowest pressures, typically involves large deflections and bending of the membrane as dents are smoothed out in forming an initial seal against the micropipet. Regime #2 involves extension and shear of the membrane into the micropipet and is accompanied by circumferential, "hoop" contraction[31] which likely initiates radial corrugations or folds that are most evident in fluorescence and brightfield imaging (Figure 3B upper inset, 3C). As explained, the buckling in this region would tend to stiffen against bending and should flatten the membrane. The highest pressure regime #3 invariably appears to smooth out some of the corrugations and likely involves direct dilational work on the covalently cross-linked network, despite no measurable change in surface density along an aspirated fluorescent projection.

With the above physics in mind, the slopes, $d\tau/dx|_i$ for each regime of aspiration provide respective measures of effective moduli. As suggested, $d\tau/dx|_2$ is related to the in-plane shear modulus, μ_{2D}. For a pipet radius (R_p) that is smaller than half the effective radius of the aspirated vesicle (R_v), a simple overall measure for extensional strain is the relative aspirated length, $x \equiv L/R_p$, that results from the imposed effective tension, $\tau = \Delta P/2R_p$. Despite the fact that the strains are large, and not infinitesimal, the in-plane shear modulus is very well approximated by $\mu_{2D} \approx d\tau/dx$.[29] Continuum computations for aspiration of an initially flat, incompressible membrane as described elsewhere[29] are readily generalized to an initially curved membrane and show that μ_{2D} is proportional to $d\tau/dx$ within a factor of about 1.2−1.4. For regime #2 (Figure 3B) detailed analyses yield $\mu_{2D} \approx 80 - 120$ mN/m.

Regime #3 provides a measure of the effective dilational resistance: specifically, $d\tau/dx|_3$ is related to a nominal K_a. Within a factor of about two and provided shear is neglected, one can show that $K_a \approx 20\ d\tau/dx|_3$ in the experimentally relevant range of R_v/R_P ($\approx$ 1.2−3).[29] For the cross-linked membranes, length increments with pressure changes are extremely small and imply that $K_a \gg 10^2$ mN/m. At full cross-linking this is

severalfold higher or more than the K_a for the uncross-linked **OB2** membrane. In addition, the post-cross-linking effective K_a is also severalfold higher than the apparent shear rigidity of regime #2, consistent with a positive Poisson ratio for a solidlike membrane.

Further comparisons with the red cell membrane prove insightful. As explained, the cross-linked spectrin network of the red cell is coupled to a bending-resistant bilayer[30] and exhibits a buckling response in aspiration, like that seen at high pressures with polymersomes here. Preceding this regime of red cell aspiration, however, is an intermediate regime where the spectrin cytoskeleton is strongly stretched in the direction of the pipet axis.[29,31] Despite the phenomonological comparisons, a spectrin network with a shear modulus of ~0.01 mN/m is obviously much softer than the fully cross-linked **OB2** membrane. The difference undoubtedly reflects the comparatively higher density of cross-links, ϕ_X. Nonetheless, the three-dimensional modulus approximated as $\mu_{3D} \approx \mu_{2D}/d$, is at the upper end of reported measures for the elastic modulus of extensively cross-linked polybutadiene. The elasticity thus appears consistent with a highly efficient cross-linking reaction that is not limited by diffusion or damage by free radicals.

Cross-Linking Efficiency. A projected density of cross-links, ϕ_X, relates to the shear elasticity via $\phi_X = k_BT/\mu_{2D}$ according to rubber elasticity theory.[32,33] The number of *lateral* cross-links per copolymer is then $n_{LAT} = {}^1/_2\ \phi_X\ A_C$. The factor of $^1/_2$ reflects a symmetric bilayer of diblocks[16] and A_C represents a projected area per copolymer chain. The minimal area can be estimated from the thickness d, the mass density of bulk PBD, and account for a bilayer structure,[16] which altogether yield: $2M_N/\rho_{PBD}\ d \approx 1\ \text{nm}^2$. Note that meandering of a chain outside of its 'box' gives an overlap with neighboring chains: the maximal area for **OE7**[34] can be as high as 2.5 nm^2 which yields an overlap of linear extent $(2.5\ \text{nm}^2/1\ \text{nm}^2)^{1/2} = 1.6$. This implies that contact interactions with *second* neighbor chains will be frequent. Given the projected area range, the number of *lateral* cross-links per copolymer is calculated to be 12−31. Provided the same density of cross-links acts to interconnect the two lamellae, the number of interlamellar or *vertical* cross-links per copolymer is estimated as $n_{VERT} \approx d^{-1}\ (A_C/\pi)^{1/2}\ n_{LAT} \approx 1-3$. A finite interlamellar cross-linking such as this is more than enough to prevent chloroform inclusions from forming within the copolymer bilayer (Figure 2A). Moreover, an overall efficiency for intermolecular cross-linking is broadly estimated by normalizing against the number of butadiene units as $(n_{LAT} + n_{VERT})/n \approx 30-75\%$, with the higher efficiency being most consistent with measures of A_C. The remainder of reacted bonds must therefore be internal to each copolymer. The less-than-perfect efficiency underscores the importance of designing in "redundant" chain reactivity.

Rigidity Percolation through a Nano-Stack. The tightly interconnected nature of the cross-linked **OB2** membrane as well as its obvious integrity as a permeability barrier (Figure 1C) reinforce the idea of a close-packed arrangement of copolymers. In projection, this translates into a hexagonal arrangement of copolymers skeletonized as a triangular lattice (Figure 4A upper inset). Within this (initially) liquid crystalline lattice, a simple topological model emerges for the cross-linking that governs the elastic stretching response: the depth d is proposed to be divided into N_{elas} layers such that, within each layer, each copolymer participates in six cross-links with its neighbors. For a triangulated network of polymer tethers, μ is proportional to the average effective elastic constant of constituent tethers or springs.[35] Projecting onto a plane a finite stack of N_{elas}, such a network tethers or springs, in register, is equivalent to summing up the springs in parallel. The effective elastic spring constant, k, is then simply related to the effective elastic constant in each layer through: $k = N_{elas}\ k_{LAYER}$. Random elimination of tethers, with the projected network still intact, will result in a continuous, linear reduction of k, and thus μ. Similar linear scaling should apply to rupture processes since tether forces are also proportional to k_{LAYER}. The number of layers per lamellae is then given by $^1/_2\ N_{elas} = n_{LAT}/6 \approx 2-5$.

Although the linearity of the rupture energy with respect to the mole fraction of the polymerizable component is consistent with rubber elasticity theory, the extrapolated offset by a critical fraction $X_C = 16 \pm 2\%$ appears nontrivial. For a triangulated network of central force interactions, a rigidity percolation limit of $p_C = {}^2/_3$ is readily derived by mean-field arguments:[36,37] most simply, one of three legs removed from a triangle is sufficiently destabilizing. Combining such destabilization with the extensive cross-linking along each polybutadiene segment suggests a stack of bond-depleted networks. Each BD block is viewed as perforating N_C layers, thereby forming a node in a stack of triangulated networks (Figure 4A inset). Progressively severing all but 6 of the $6N_C$ elastic tethers emanating from each copolymer, the stack is expected to exhibit a linear decrease in its elastic constants as it is reduced in projection to a single triangulated network. Further dilution also leads to a linear decrease in the elastic constants, within mean-field theory, down to the critical fraction

$$X_C = p_C\ (6/6\ N_C) \tag{1}$$

For X above X_C, the membrane is solidlike, and for X well below X_C the membrane is fluidlike; these expectations are confirmed by fluorescence photobleaching experiments reported elsewhere.[38] Note that the dependence of X_C on lattice-connectivity is manifested *only* in the prefactor, p_C, and thus reduces the sensitivity to the presumed close-packed, quasi-hexagonal symmetry. Solving eq 1 yields $N_C = 4-5$ which is in very good agreement with N_{elas} despite the very different mean-field physics. The vision of stacked percolating networks is fortified below by measures of the dependence of the membrane rupture tension, τ_R, on X above X_C.

Membrane Cracking for $X \gg X_C$. Between X_C and the fully cross-linked limit, the rupture stress is found to scale approximately as $(X - X_C)^\beta$, $\beta \approx 1.48$. This will be shown largely consistent with a simplified, planar form of Griffith crack theory, where interface energy competes against bulk energy. In terms of suitable D-dimensional parameters and fields,[39] the cost of forming a rupture interface of energy density γ_R is balanced against the elastic stress energy, $\sim\sigma_R^2/\mu_D$, that is relieved upon rupture. Note that, for $D = 2$, γ_R has units of energy per length and $\sigma_R \equiv \tau_R$. For a so-called penny crack of width w in D-dimensions, the rupture energy is $\epsilon_R = \gamma_R\ w^{D-1}$, and the total free energy, ignoring constants, has the form $F \approx \gamma_R\ w^{D-1} - \sigma_R^2/\mu_D\ w^D$. Minimization with respect to w yields

$$\sigma_R = \text{constant} \times (\epsilon_R \mu_D / w^D)^{1/2} \tag{2}$$

Although $\epsilon_R \sim (X - X_C)^{D-1}$ is reasonably intuitive, rubber elasticity theory suggests and Figure 3C confirms (for $D = 2$ at least) that $\mu_D \sim (X - X_C)^1$. Furthermore, a simple scaling for the crack width is given by the average inter-nodal spacing of the cross-linked structure as $w \sim (X - X_C)^{-1/D}$. Combining these separate scaling relations yields $\sigma_R \approx (X - X_C)^\beta$, where $\beta = (D+1)/2$. Clearly, $D = 2$ fits the experiments and confirms

that the cross-link-dependent rupture tension reflects a small number of layered-cross-links compared to the large number being stressed.

Chains of Cross-Linked OB2 in a Homogeneous Fluid of OE7 for $X < X_c$. The rupture tension was found to be a minimum at a measured value of 10 mN/m near $X \equiv X^* =$ 10%. Interestingly, the decrease in τ_r from $X = 0$ to X^* is linear ($R^2 = 0.997$) with a slope of (1 mN/m) per $\%X_{OB2}$. Within this same range, Figure 4A suggests that the membrane is overall fluid, devoid of any shear elasticity. Furthermore, the noted lack of any optically resolvable domain structure (with fluorescently tagged copolymer) suggests a homogeneous phase. On the basis of these results for $0 \leq X \leq X^*$, we propose a solid-in-fluid nanophase that has a lateral interface between the two phases which facilitates or nucleates rupture. The incompatibility which emerges could well reflect cross-link-strain[2] induced mismatch of hydrophobic core thicknesses. Because this interface evidently grows in linear proportion to cross-linked mass, linear or ramified chains of cross-linked copolymer are implicated as opposed to tight, separated domains. This picture is certainly consistent with the initially high miscibility between **OB2** and **OE7**. Moreover, as these chains begin to percolate across the entire surface as X increases from 0 to X_c, the elastic rigidity and toughness ought to suddenly increase, just as found (Figure 4). Most dramatic perhaps is the rapid rise in τ_r that is sketched between $\approx$10−15% **OB2** (i.e., X^* and X_c) and is highly suggestive of critical phenomena. Although focused on copolymer, the mechanism suggested here highlights the limitations of polymerizable lipids with minimal reactivity as well as the importance of intrinsic membrane robustness.

Summary

Covalent cross-linking of nano-structures that self-assemble in solution is rapidly emerging as a way of making permanent what is, by definition, labile. However, establishing the efficiency as well as the physical effects of cross-linking is not trivial at such scales. It is nonetheless important because intermolecular polymerization competes, unsuccessfully if the reactivity is limited, against intramolecular bond formation as well as other mechanisms of termination. Stability tests reported here for a polymer membrane provide very direct evidence of thorough and durable cross-linking over length-scales of microns. Because defects as small as a sucrose molecule would be rapidly revealed through permeation and stress-sensitive rupture, the proof here appears robust. What is thus most clear is that efficient cross-linking is possible and tunable through blending at the nanoscale, with dramatic effects on strength and durability and a definitive transition from interface-dominated properties to cross-link-dominated. In addition, such structure-constrained cross-linking inspires new views of phenomena such as rigidity percolation in reduced dimensionality systems.

Acknowledgment. We thank M. Santore (Lehigh) for fluorescently labeled copolymer and James C-M. Lee for fluorescence imaging. This work was supported by NSF-MRSEC grants to Penn and U. Minn. as well as a NASA grant.

References and Notes

(1) Liu, G. J.; Qiao, L. J.; Guo, A. *Macromolecules* **1996**, *29*, 5508−5510.
(2) Won, Y.-Y.; Davis, H. T.; Bates, F. S. *Science* **1999**, *283*, 960−963.
(3) Thurn-Albrecht, T.; Schotter, J.; Kästle, G. A.; Emley, N.; Shibauchi, T.; Krusin-Elbaum, L.; Guarini, K.; Black, C. T.; Tuominen, M. T.; Russell, T. P. *Science* **2000**, *290*, 2126−2129.
(4) Doshi, D. A.; Huesing, N. K.; Lu, M.; Fan, H.; Lu, Y.; Simmons-Potter, K.; Potter, B. G., Jr.; Hurd, A. J.; Brinker, C. J. *Science* **2000**, *290*, 107−111.
(5) Lipowsky, R.; Sackmann, E. Eds. *al Physics*; Elsevier Science: Amsterdam, 1995; Vol. 1.
(6) Dorn, K.; Klingbiel, R. T.; Specht, D. P.; Tyminski, P. N.; Ringsdorf, H.; O'Brien, D. F. *J. Am. Chem. Soc.* **1984**, *106*, 1627−1633.
(7) Fendler, J. H. *Science* **1984**, *223*, 888−894.
(8) Sisson, T. M.; Lamparski, H. G.; Kolchens, S.; Elayadi, A.; O'Brien, D. F. *Macromolecules* **1996**, *29*, 8321−8329.
(9) Okada, J.; Cohen, S.; Langer, R. *Pharm. Res.* **1995**, *12*, 576−582.
(10) Meier, H.; Sprenger, I.; Barmann, M.; Sackmann, E. *Macromolecules* **1994**, *27*, 7581−7588.
(11) Mutz, M.; Bensimon, D.; Brienne, M. J. *Phys. Rev. Lett.* **1991**, 923−926.
(12) Komatsu, T.; Tsuchida, E.; Böttcher, C.; Donner, D.; Messerschmidt, C.; Siggel, U.; Stocker, W.; Rabe, J. P.; Fuhrhop, J.-H. *J. Am. Chem. Soc.* **1997**, *119*, 11 660−11 665.
(13) Liu, S.; O'Brien, D. F. *Macromolecules* **1999**, *32*, 5519−5524.
(14) Cornelissen, J. J. L. M.; Fischer, M.; Sommerdijk, N. A. J. M.; Nolte, R. J. M. *Science* **1998**, *280*, 1427−1430.
(15) Nardin, C.; Hirt, T.; Leukel, J.; Meier, W. *Langmuir* **2000**, *16*, 1035−1041.
(16) Discher, B. M.; Won, Y. Y.; Ege, D. S.; Lee, J. C. M.; Bates, F. S.; Discher, D. E.; Hammer, D. A. *Science* **1999**, *284*, 1143−1146.
(17) Discher, B. M.; Hammer, D. A.; Bates, F. S.; Discher, D. E. *Curr. Opin. Colloid Interface Sci.* **2000**, *5*, 125−131.
(18) Gittes, F.; MacKintosh, F. C. *Phys. Rev. E* **1998**, *58*, R1241−R1244, Part A.
(19) Schmid-Schonbein, H.; Heidtmann, H.; Grebe, R. *Blut.* **1986**, *52*, 131−47.
(20) Gaub, H.; Buschl, R.; Ringsdorf, H.; Sackmann, E. *Chem. Phys. Lipids* **1985**, *37*, 19−43.
(21) Lobkovsky, A.; Gentges, S.; Li, H.; Morse, D.; Witten, T. A. *Science* **1995**, *270*, 1482−1485.
(22) Israelachvili, J. In *Intermolecular and Surface Force*, 2nd ed.; Academic Press: New York, 1991.
(23) Hillmyer, M. A.; Bates, F. S. *Macromolecules* **1996**, *29*, 6994.
(24) Helfand, E.; Wasserman, Z. R. In *Developments in Block Copolymers*; Applied Science: New York, 1982; Chapter 4.
(25) Bloom, M.; Evans, E.; Mouritsen, O. G. *Q. Rev. Biophys.* **1991**, *24*, 293.
(26) Lee, J. C.-M.; Bermudez, H.; Discher, B. M.; Sheehan, M. A.; Won, Y.-Y.; Bates, F. S.; Discher, D. E. *Biotech. Bioeng.* **2001**, *43*, 135−145.
(27) Importantly, Won et al. showed by small angle neutron scattering that the BD core of wormlike micelles was reduced in radius by about 10% when cross-linked. This is not resolvable by cryo-TEM, but, for an incompressible core, such a reduction translates into an area dilation per molecule of about 10%.
(28) Landau, L. D.; Lifshitz, E. M. In *Theory of Elasticity*, 3rd ed.; Pergamon Press: Oxford, 1986.
(29) Evans, E. A.; Skalak, R. In *Mechanics and Thermodynamics of Biomembrane*; CRC Press: Boca: Raton, Fla., 1980.
(30) Evans, E. A. *Biophys. J.* **1983**, *43*, 27−30.
(31) Lee, J. C.-M.; Wong, D.; Discher, D. E. *Biophys. J.* **1999**, *77*, 853−864.
(32) Stokke, B. T.; Mikkelsen, A.; Elgsaeter, A. *Biophys. J.* **1986**, *49*, 319−327.
(33) Treloar, L. R. G. In *The Physics of Rubber Elasticity*, 3d ed.; Clarendon Press: Oxford, 1975.
(34) Hajduk, D. A.; Kossuth, M. B.; Hillmyer, M. A.; Bates, F. S. *J. Phys. Chem. B* **1998**, *102*, 4269−4276.
(35) Discher, D. E.; Boal, D. H.; Boey, S. K. *Phys. Rev. E* **1997**, *55*, 4762−4772.
(36) Feng, S.; Sen, P. N. *Phys. Rev. Lett.* **1984**, *52*, 216−219.
(37) Thorpe, M. F.; Garboczi, E. J. *Phys. Rev. B* **1987**, *35*, 8579−8586.
(38) Lee, J. C−M.; Santore, M.; Bates, F. S.; Discher, D. E. *Macromolecules* **2001**,.
(39) Arndt, P. F.; Nattermann, T. *Phys. Rev. B* **2001**, *6313*, 4204.